Resting-state is not enough: alpha and mu rhythms change shape across development, but lack diagnostic sensitivity

Andrew Bender[1], Bradley Voytek*[1,2,3,4], and Natalie Schaworonkow*[5]

[1]Neurosciences Graduate Program,
[2]Department of Cognitive Science,
[3]Halıcıoğlu Data Science Institute,
[4]Kavli Institute for Brain and Mind, University of California, San Diego, La Jolla, CA, USA.
[5]Ernst Strüngmann Institute for Neuroscience, Frankfurt am Main, Germany
* *contributed equally to the work*

In the human brain, the alpha rhythm in occipital cortex and the mu rhythm in sensorimotor cortex are among the most prominent rhythms, with both rhythms functionally implicated in gating modality-specific information. Separation of these rhythms is non-trivial due to the spatial mixing of these oscillations in sensor space. Using a computationally efficient processing pipeline, we show that alpha and mu rhythms can be separated from electroencephalography recordings performed on nearly 3000 children aged 5–18. Using the extracted time series for each rhythm, we characterized the waveform shape on a cycle-by-cycle basis and examined whether and how the waveform shape differs across development and in attention-deficit hyperactivity disorder (ADHD) and autism spectrum disorder (ASD). Alpha and mu rhythms both exhibit nonsinusoidal waveform shape that changes significantly across development. We found no differences in the resting-state features of these alpha-band rhythms for either ADHD or ASD in comparison to typically developing participants. While waveform shape is ignored by traditional Fourier spectral analyses, these nonsinusoidal properties may be informative for building more constrained generative models for different types of alpha-band rhythms. Our results highlight the difficulties in identifying targeted biomarkers for ADHD and ASD from resting-state alpha-band rhythms.

Introduction

Rhythms in the alpha band (8–13 Hz) are the most prominent rhythms in the human brain (Klimesch, 2012). The occipital alpha rhythm is most noticeable during wakeful periods when participants' eyes are closed (Berger, 1929), but also changes dynamically during attentional tasks, decreasing in brain areas related to task-specific visual input (Kelly et al., 2006; Thut et al., 2006; Worden et al., 2000). By contrast, the sensorimotor mu rhythm is strongest when a participant is not moving (Salmelin and Hari, 1994). Mu activity changes dynamically during motor tasks, decreasing in power in motor areas controlling moving body parts and increasing in power in motor areas controlling immobile body parts (Pfurtscheller and Neuper, 1994). In this way, both alpha and mu rhythms are important for gating modality-specific information, inhibiting the processing of functionally irrelevant information.

These rhythms share a frequency band and display a similar change in frequency across development, one of the strongest effects in the field of oscillations (Freschl et al., 2022; Lindsley, 1939). Despite this, the rhythms show distinct waveform shape: alpha rhythms appear triangular in raw traces (Stam et al., 1999), while mu rhythms are considered to have an arc-shaped waveform (Gastaut and Bert, 1954; Kuhlman, 1978). The waveform shape likely reflects differences in the physiological properties of the underlying oscillatory generators (Cole and Voytek, 2017). Computational modeling has suggested that the sharpness of oscillatory peaks and troughs reflects the synchronicity of the underlying excitatory input currents (Sherman

et al., 2016). The waveform shape of alpha and mu rhythms have not yet been characterized in developmental populations. With the main factor driving the prominent oscillatory frequency increase during development remaining unknown, such precise characterization will help determine whether the oscillatory changes are driven by gross anatomical changes or distinct modifications to the oscillatory generators underlying these rhythms.

Given the strong changes in oscillations across development and the link of waveform shape to pathophysiological properties of circuits in Parkinson's disease (Cole, van der Meij, et al., 2017), we were interested in whether the waveform shape of resting-state alpha and mu rhythms acquired in a developmental population could serve as a biomarker. Alpha-band rhythms have been implicated in autism spectrum disorder (ASD) and attention deficit hyperactivity disorder (ADHD) in terms of both their frequency and power, though the results have been inconsistent and/or mixed (Freschl et al., 2022; Javitt et al., 2020).

The aim of the current study was therefore twofold: we investigated how waveform shape features of alpha and mu rhythms change both across development and neurodevelopmental disorders. Our study provides three methodological advantages over existing approaches. First, we analyze the signals primarily in the time domain (Cole and Voytek, 2019), to characterize nonsinusoidal features of these rhythms. Second, we use a large open developmental dataset (ages 5–18) of high density, resting-state electroencephalography (EEG) (Alexander et al., 2017), allowing us to perform a high-powered comparison of alpha and mu rhythms across development. Third, we use spatio-spectral decomposition (SSD) (Nikulin, Nolte, and Curio, 2011), a statistical procedure using individual peak frequency information to isolate alpha and mu rhythms that are mixed on the sensor level due to EEG volume conduction (Schaworonkow and Nikulin, 2022).

We found that, while both alpha and mu are nonsinusoidal, mu rhythms have a significantly higher peak-trough asymmetry compared to alpha. Although alpha and mu rhythms are very similar in their frequency, this confirms that these rhythms can be differentiated on a cycle-by-cycle basis using their waveform shape. Additionally, we found that both alpha and mu rhythms increase in frequency and amplitude across development while becoming more nonsinusoidal. We further demonstrated that the two rhythms change differentially across age. Still, accounting for the significant changes in waveform features across development, we find no significant difference in waveform features for ADHD or ASD in comparison to typically developing participants, suggesting that no sensitive biomarkers can be constructed from these features of resting-state alpha-band rhythms.

Results

Methodological approach for establishing the presence of alpha and mu rhythms

Our processing pipeline aimed for a computationally efficient investigation of EEG alpha-band rhythms in a dataset of nearly 3000 minors aged 5–18, consisting of approximately 5 minutes of resting-state activity in 128 channels (Fig. 1A). Our focus was specifically occipital alpha rhythms and sensorimotor mu rhythms. First, we identified the peak frequency in a broad, 6–13 Hz range in two occipital and two sensorimotor channels for each participant using the spectral parameterization method (Donoghue et al., 2020) (Fig. 1B). We then used each individual's average alpha-band peak frequency across the four channels to seed a spatial filtering algorithm called spatio-spectral decomposition (SSD) that extracts oscillatory sources with high alpha-band signal-to-noise ratio (SNR). Each extracted source consisted of a time series and associated spatial topography (Fig. 1C). Using a template magnetic resonance image developed

specifically for a developmental population (Fonov et al., 2011), we used a template matching approach to estimate the source location that best accounts for the spatial pattern of the strongest components with high alpha-band SNR for each participant (Fig. 1D). The spatial patterns were compared to 32,772 source location lead fields using a distance metric. The majority of sources were localized to occipital and sensorimotor cortices after imposing alpha-band SNR and acceptable pattern distance thresholds (Fig. 1E). We classified the SSD components with SNR > 5 dB located in the occipital cortex as alpha rhythms (Fig. 1E-F, purple) and those located in sensorimotor cortices as mu rhythms (Fig. 1E-F, green). Because of these constraints, we were not able to identify both alpha and mu rhythms for every participant. Our extraction procedure resulted in sensorimotor mu rhythms for 13.0% (387/2969) of participants and visual alpha rhythms for 45.4% (1348/2969) of participants (Fig. 1F). These numbers also reflect the challenging data quality of a developmental EEG dataset. The time series for these selected high-SNR alpha and mu rhythms were then used for all subsequent waveform shape analyses.

Alpha and mu rhythms differ in their oscillatory waveform features

After extracting alpha and mu rhythm time series (example seen in Fig. 2A), we computed waveform features on a cycle-by-cycle basis, using the same approach as (Cole and Voytek, 2019). Each time series was divided into cycles by identifying zero crossings and extrema (peaks and troughs) for each cycle of the alpha-band rhythm. A cycle was classified as a burst after passing burst detection criteria (see Methods). We quantified four waveform features: average frequency, rise-decay asymmetry, peak-trough asymmetry, and amplitude (see Fig. 2B). The oscillation frequency was computed as the inverse of the cycle period. We assessed the asymmetry of the time series with two different metrics, using the rise-decay asymmetry as well as the peak-trough asymmetry; the former measures the asymmetry in the amount of time spent in the oscillation cycle rise versus decay, whereas the latter measures the amount of time spent in the oscillation peak compared to the trough, approximating the "sharpness" of the cycle extrema. Normalized amplitude was computed as the ratio between the amplitude of the burst vs. non-burst cycles. This measure strongly correlates with the 1/f-corrected spectral peak alpha-band amplitude ($r = 0.83$), but can be calculated from the time series.

We assessed all measures within as well as across participants, as both types of rhythms could not be extracted for every participant. The comparison of alpha and mu waveform features between participants are shown in Fig. 2C: alpha peak frequency was lower than mu peak frequency ($t = -4.28$, $d = -0.235$, $p = 0.000172$). Additionally, mu rhythms were more asymmetrical than alpha rhythms in both measures of asymmetry: rise-decay asymmetry ($t = -4.81$, $d = -0.312$, $p = 1.55 \cdot 10^{-5}$) and peak-trough asymmetry ($t = -11.5$, $d = -0.968$, $p = 4.96 \cdot 10^{-26}$). Normalized amplitude was higher for alpha rhythms ($t = 13.6$, $d = 0.625$, $p = 7.07 \cdot 10^{-38}$), reflecting burst cycles of higher magnitude. Within participants, waveform features showed the same alpha/mu differences as between participants, such that alpha rhythms showed lower peak frequency, less asymmetry, and were of higher amplitude than mu rhythms (Fig. 2D). Effect sizes within participants were also of similar magnitude to those across participants. This shows that effects seen across the population are also generally reflected within individuals.

In summary, the results indicate that our analysis pipeline was able to extract differential alpha and mu rhythm waveform characteristics efficiently in a large dataset, in line with qualitative descriptions in previous literature.

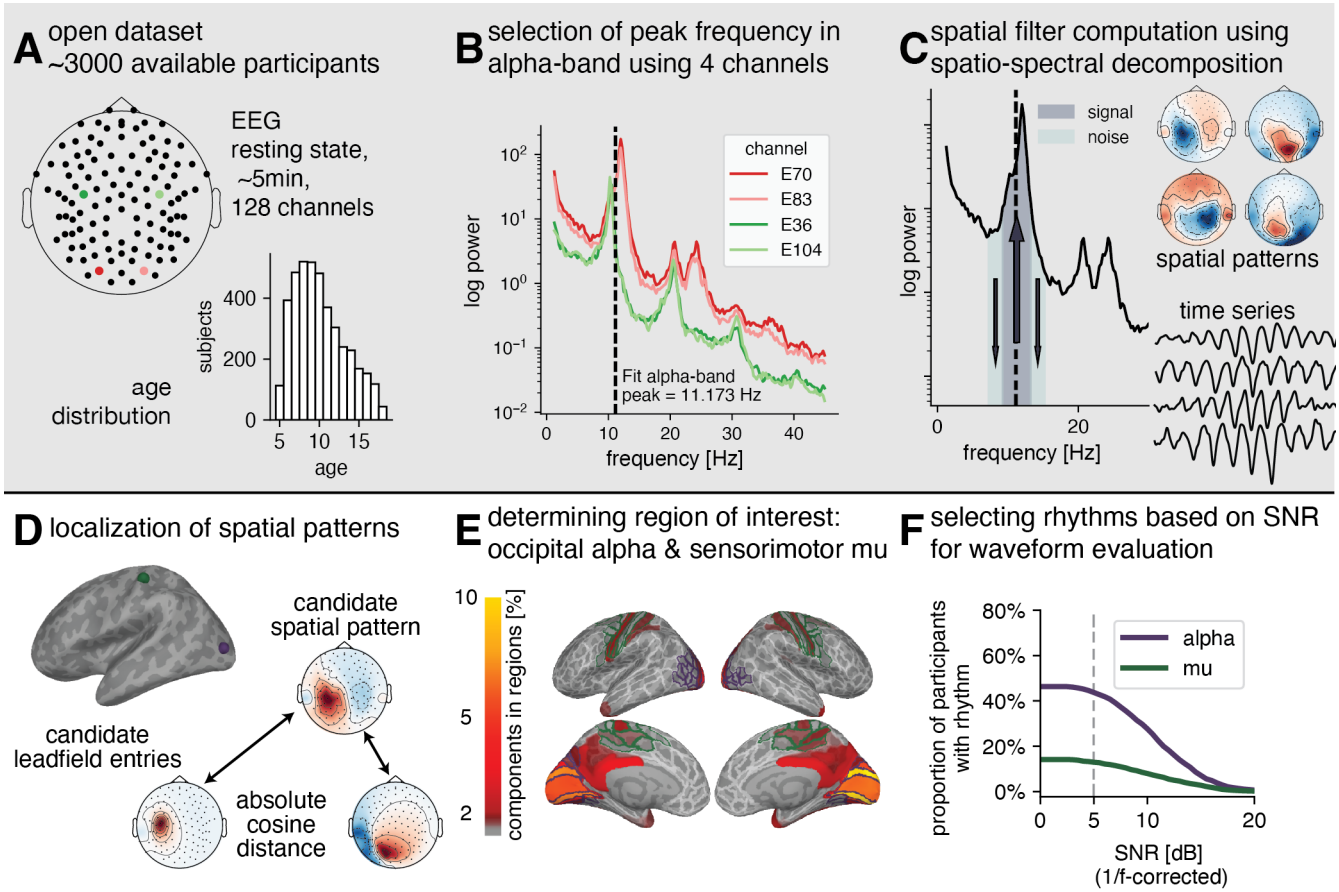

Figure 1: Analysis pipeline for extracting occipital alpha and sensorimotor mu rhythms with high SNR in a large developmental EEG dataset. (A) Sensor positions of 128-channel EEG (left) and the distribution of ages (bottom right) within the dataset. (B) Power spectra for two occipital channels (red) and two sensorimotor channels (green) for one participant in order to estimate the average alpha-band peak frequency across the four channels (black dashed line). (C) The spatial filtering algorithm SSD extracts oscillatory sources with high alpha SNR by maximizing power within the defined frequency band of interest and minimizing power within defined neighboring frequency bands (left), with each source characterized by its spatial distribution (top right) and time series (bottom right). (D) To localize sources, the absolute cosine distance was computed for each SSD spatial pattern and lead field entry for each possible location. (E) Heat map of locations of the extracted alpha-band components superimposed on a 3D brain, for an SNR threshold of 5 dB and a pattern distance metric of 0.15. Components localized to an occipital region (outlined in purple) were classified as alpha components, while components localized to a sensorimotor region (outlined in green) were classified as mu components. (F) The percentage of participants who had a detectable rhythm exceeding a specified SNR threshold for alpha and mu rhythms, respectively.

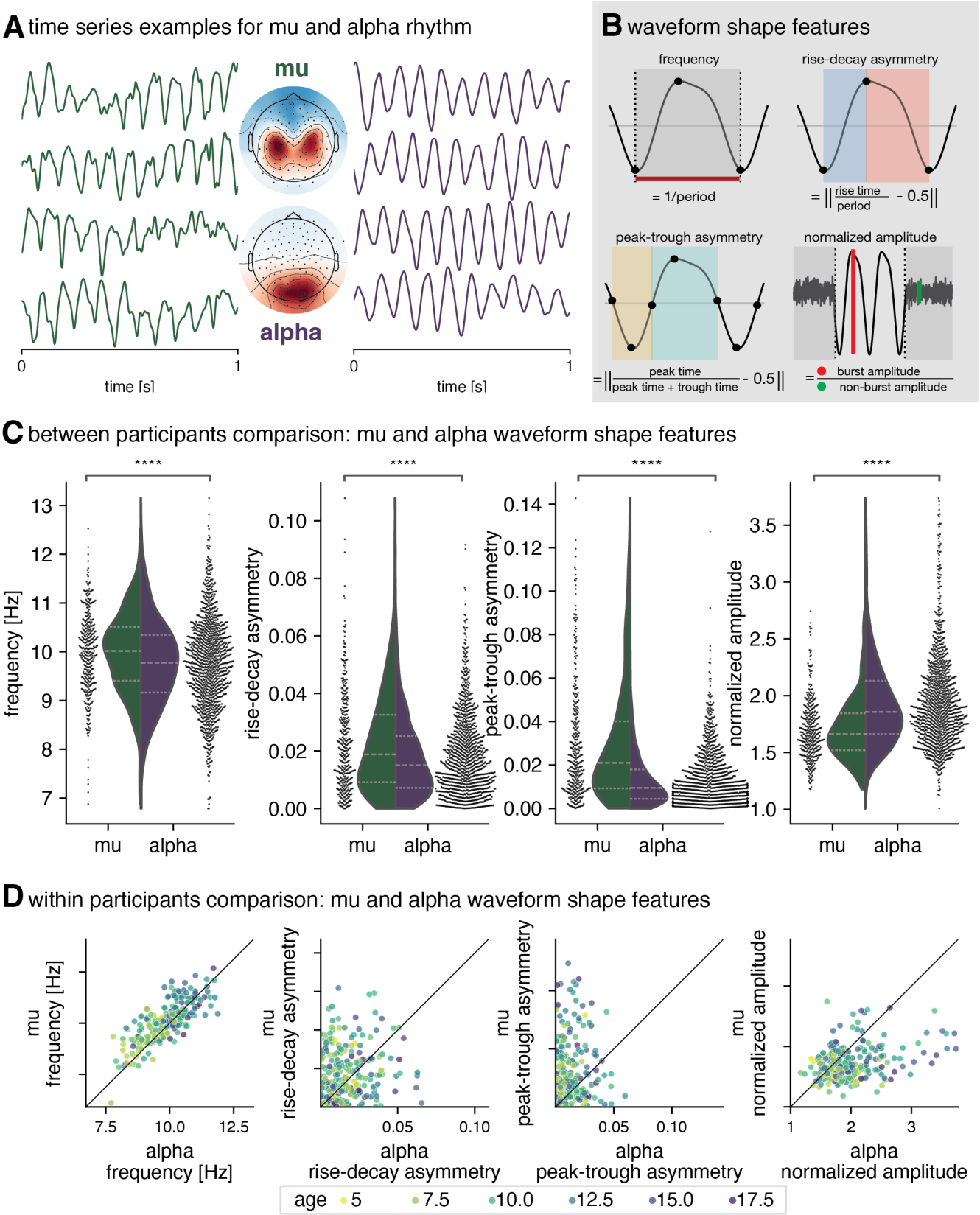

Figure 2: Waveform features differ between alpha and mu rhythms. (A) Example time series for alpha and mu components from two participants. The topoplot inset shows the average topography for each rhythm type. (B) Assessed waveform features: frequency, rise-decay asymmetry, peak-trough asymmetry, and normalized amplitude. (C) Mean waveform features for extracted alpha rhythms (purple) and mu rhythms (green) across participants (N=1507). (D) Mean waveform features within participants (N=228) in which both components could be identified. Deviations from the diagonal are indicative of a significant difference between the waveform features within participants.

Waveform features differ strongly across development

After evaluation of waveform shape features for each rhythm type, we next investigated how these waveform shape features change across development. The results are shown in Fig. 3A. First, we reproduced the classic increase of frequency across development for both alpha ($r = 0.521$, $p = 1.18 \cdot 10^{-80}$) and mu ($r = 0.368$, $p = 5.98 \cdot 10^{-12}$). Second, mu rise-decay asymmetry decreases significantly across development ($r = -0.154$, $p = 0.0159$), while alpha does not show a significant increase ($r = 0.0536$, $p = 0.275$). For peak-trough asymmetry, both rhythm types display increasing nonsinusoidality with higher age (alpha: $r = 0.187$, $p = 6.09 \cdot 10^{-10}$; mu: r=0.195, $p = 1.1 \cdot 10^{-3}$). Additionally, we showed that both alpha ($r = 0.229$, $p = 1.28 \cdot 10^{-14}$) and mu ($r = 0.222$, $p = 1.23 \cdot 10^{-4}$) increase in burst amplitude relative to non-burst cycle amplitude across development.

To compare the relationship between waveform features and age across the two rhythm types in a more fine grained way, we estimated linear models using resampling and permutation statistics. We formulate a linear model for each rhythm type in which each feature is a function of age: feature = $\beta_1 \cdot \text{age} + \beta_0$. To determine whether there are distinct slopes and offsets for mu and alpha rhythms in their relationship with age, we performed resampling with replacement of feature values and fit linear models to the resampled feature values across age for both rhythm types to calculate p-values (results are reported as 95% confidence intervals of the difference between alpha and mu parameters, in square brackets). Our results show that the two rhythm types change differentially across age (see Fig. 3B for slope and Fig. 3C for intercept). The slope differences indicate that changes in rhythm characteristics across development affect one rhythm more than the other. Alpha changes across development were more pronounced than those for for mu in frequency ([0.0228, 0.0811], $p = 0.004$), rise-decay asymmetry ([0.0003, 0.0015], $p = 0.0056$), and amplitude ([0.0061, 0.0294], $p = 0.0026$), while changes in peak-trough asymmetry were more pronounced for mu than alpha ([-0.002, -0.001], $p = 0.0258$). The difference in intercept indicates that the changes in rhythm characteristics are already evident at the beginning of the age range in this study (minimum age 5). Frequency ([-0.5582, -0.2092], $p < 0.0001$) and both asymmetry measures (rise-decay: [-0.013, -0.0056], $p < 0.0001$; peak-trough: [-0.0147, -0.0046], $p < 0.0001$) were higher for mu at age 5, while amplitude ([0.1064, 0.2305], $p < 0.0001$) was higher for alpha at age 5.

In this way, our procedure was able to quantify differences in waveform features separately for mu and alpha, with each rhythm type displaying unique characteristics, albeit with high individual variance. In the following section, we examine whether the individual variance can be linked to several types of clinical diagnoses.

Resting-state rhythm features across diagnoses

Given the easy applicability of resting-state EEG in a developmental population, there is substantial interest in deriving sensitive biomarkers from resting-state EEG. Therefore, we compared the above waveform shape features across clinical diagnoses to see if alpha rhythm (Fig. 4A) or mu rhythm (Fig. 4B) features could be related to ADHD or ASD diagnoses. An analysis of covariance (ANCOVA) was conducted to examine the influence of diagnosis (with three levels: ADHD, ASD, and no diagnosis) on each of the four waveform features while accounting for the covariate age, reflecting an age-matched sampling approach. The main factor of diagnosis was not significant for any of the waveform features for both alpha (frequency: $F = 3.5$, $p = 0.221$, rise-decay asymmetry: $F = 1.98$, $p = 0.291$, peak-trough asymmetry: $F = 1.93$, $p = 0.291$, and normalized amplitude: $F = 2.91$, $p = 0.221$) and mu rhythms

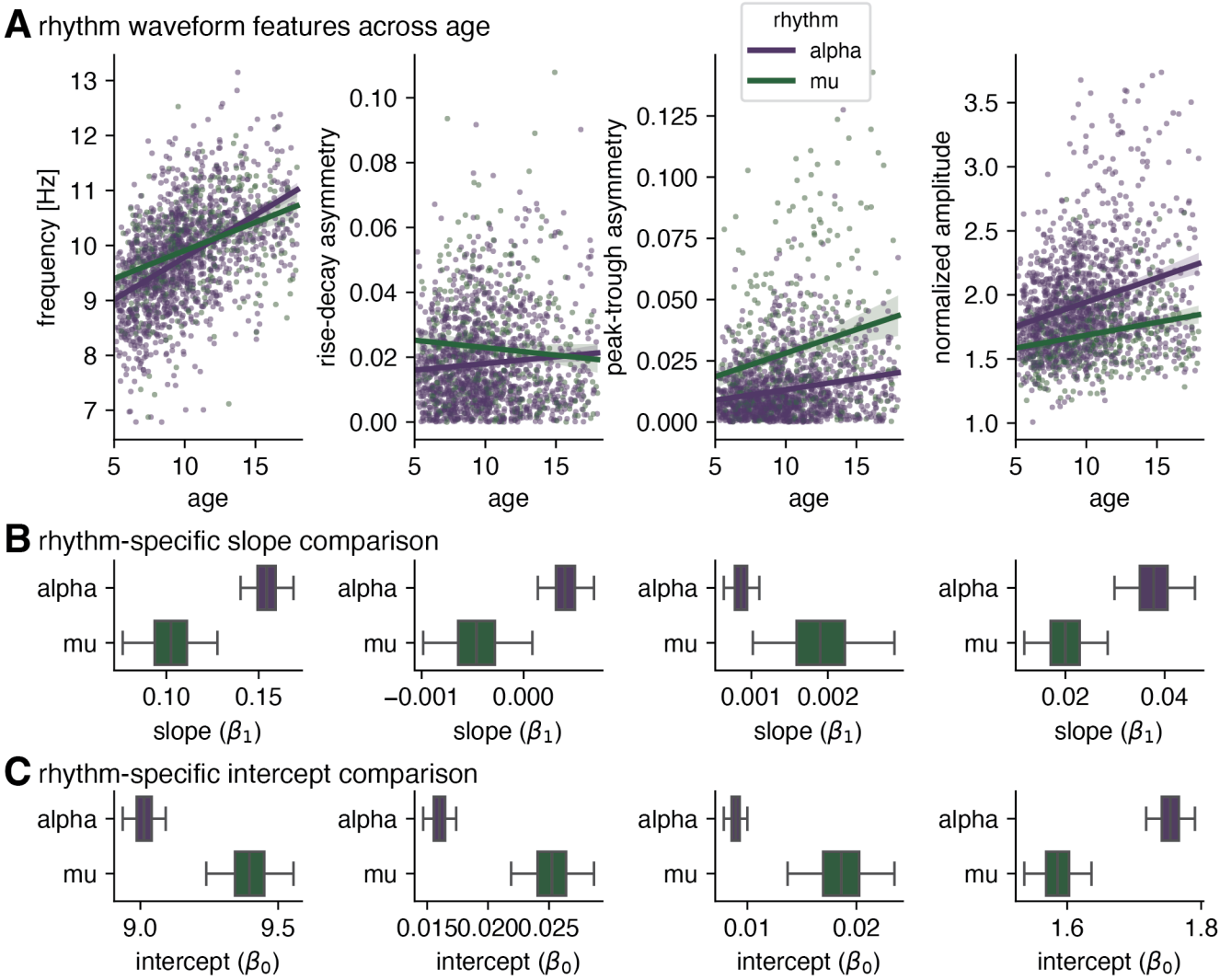

Figure 3: Alpha and mu rhythm waveform features show differential changes across development. (A) Alpha (purple) and mu (green) waveform features (frequency, rise-decay and peak-trough asymmetry, normalized amplitude) by age across participants. (B) Slope of linear model for alpha and mu rhythm. Boxes denote interquartile range and whiskers denote 95% confidence interval of bootstrapped feature values, 10,000 iterations. (C) Intercept of linear model for alpha and mu rhythm. Boxes denote interquartile range and whiskers denote 95% confidence interval of bootstrapped feature values, 10,000 iterations.

(frequency: $F = 0.243$, $p = 0.818$, rise-decay asymmetry: $F = 0.749$, $p = 0.632$, peak-trough asymmetry: $F = 1.359$, $p = 0.415$, and normalized amplitude: $F = 0.201$, $p = 0.818$). These null results were further supported by pairwise post-hoc t-tests that controlled for age. This indicates that, taking age into account, there were no significant differences in all four waveform shape features we investigated between participants with ADHD and ASD compared to typically developing participants for either alpha-band rhythm.

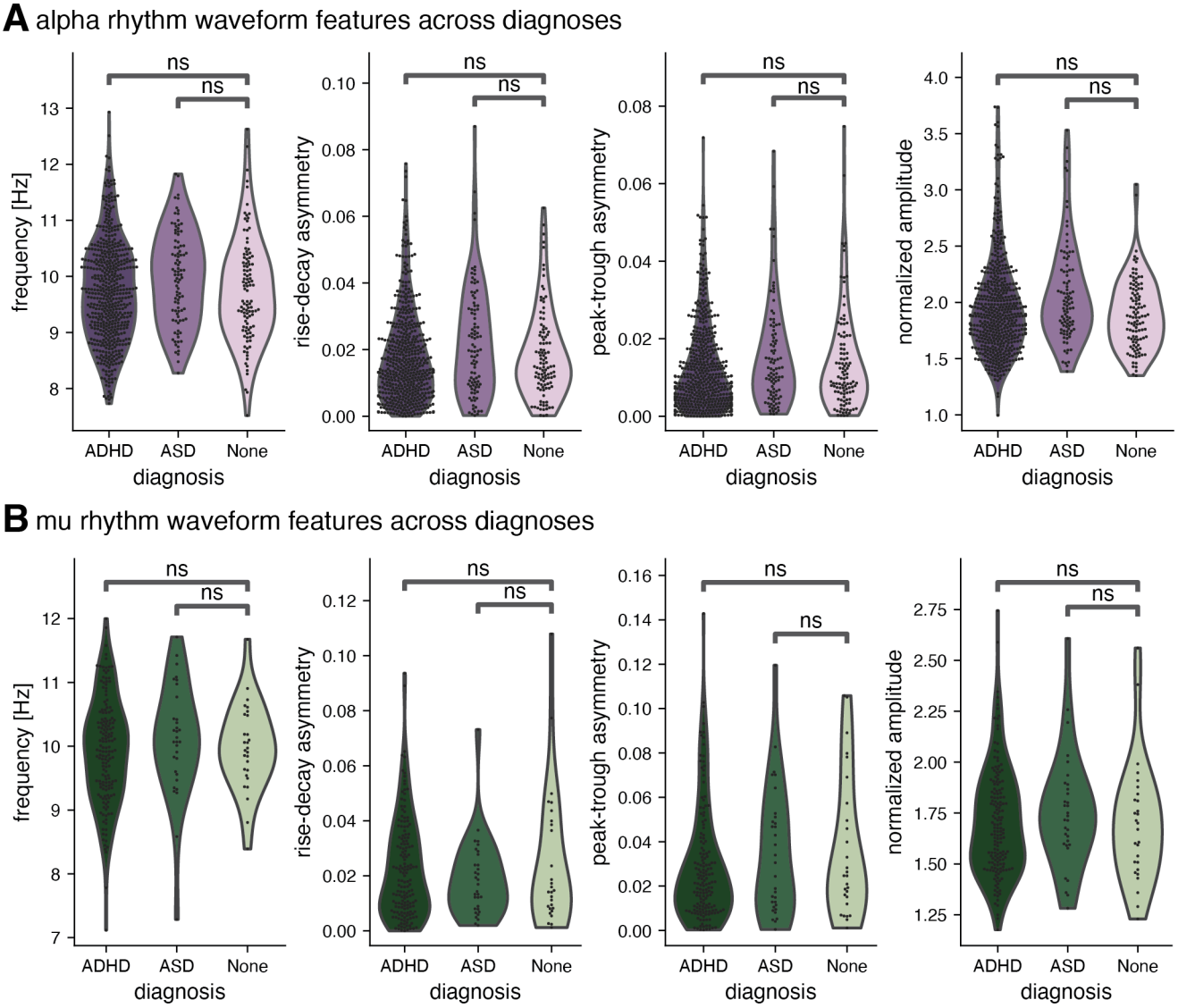

Figure 4: Resting-state alpha and mu waveform features across ADHD and ASD diagnoses compared to typically developing participants. (A) alpha rhythm components: mean waveform features (frequency, rise-decay and peak-trough asymmetry, normalized amplitude) in participants who received a ADHD and ASD diagnosis, and for participants who did not receive a diagnosis (ADHD: N=596, ASD: N=120, no diagnosis N=101). (B) mu rhythm components: mean waveform features in participants who received a ADHD and ASD diagnosis, and for participants without a diagnosis (ADHD: N=161, ASD: N=32, no diagnosis N=28). No statistically significant difference between the two disorder groups and typically developing participants was found for any waveform feature and rhythm type.

Discussion

With these analyses, we have established a data analysis pipeline to extract distinct oscillatory rhythms that overlap in frequency in resting-state EEG. The data-driven spatial filtering approach leverages the differential spatiospectral distribution of occipital alpha and sensorimotor mu to identify independent rhythms, as there could be several underlying generators that are differentially altered (Dumas et al., 2014). This approach effectively identifies components that have significant alpha power exceeding 1/f-activity and display the narrowband peak structure of neural alpha-band rhythms, in the presence of noise, reducing the need for extensive preprocessing. This approach also reduces the chance of conflation of oscillatory and 1/f-activity in this context (Cellier et al., 2021). We used these spatial filters to linearly transform the broadband activity across electrodes into component time series, enabling the quantification of waveform shape across rhythms, diagnoses, and development.

This analysis demonstrated that both occipital alpha and sensorimotor have distinct, nonsinusoidal waveform shape. We replicated long-standing findings that occipital alpha has lower frequency and higher amplitude than sensorimotor mu at a large scale (up to 1507 participants). Through our time series analysis of waveform shape, we were able to quantify the observed qualitative differences between the waveform shape of occipital alpha and sensorimotor mu. Moreover, the waveform asymmetry differences we found were much stronger than the well-established differences in frequency and amplitude, suggesting that the principal difference between these rhythms lies in the distinct asymmetries of each rhythm's stereotyped waveform. Both these rhythms show substantial changes in waveform shape across development, increasing in frequency and amplitude and becoming more nonsinusoidal. Differences in waveform features are already present at age five, and the rate at which these waveform features change across development is significantly different between alpha and mu. Despite the significant differences between the waveform shapes of alpha and mu, neither rhythm showed any statistically significant difference in waveform shape across the examined diagnoses.

Implications

A number of different modeling approaches have been employed to understand the generation of alpha-band rhythms. Quantifying the waveform shape of the distinct rhythm types that can be measured in the human EEG will aid in constraining generative models of alpha-band rhythms, for which the underlying generators are still insufficiently understood (Halgren et al., 2019). Neural mass models have been used to represent the average membrane potential and firing rate of large numbers of neurons (Lopes Da Silva et al., 1976), generating rhythmic activity similar to biologically observed alpha rhythms (Jansen and Rit, 1995). While important for understanding electrophysiological data at the level of local field potentials and EEG, these models fail to explain rhythm genesis at the level of synapses and individual neurons, which constitutes a promising target for interventions that seek to ameliorate cognitive deficits associated with these rhythms. To our knowledge, generative biophysical models for different types of alpha rhythms that take into account distinct types of waveform shape have not yet been developed. Our findings show that both alpha and mu rhythms have stereotyped, nonsinusoidal waveforms that become more asymmetrical across development. Such robust descriptive statistics will aid in the constraining of future generative biophysical models for these rhythms, which should account for these distinct waveform shapes and how they change in development.

These findings add to an already-substantial amount of studies showing that developmental

changes in oscillations are dramatic (Freschl et al., 2022), despite significant inter-individual variability in the precise timing of such changes. The structural and physiological changes that underlie these pronounced changes across development remain unknown. Understanding these structural and physiological underpinnings of alpha-band rhythms will likely be crucial for future interventions that aim to ameliorate the functional deficits that have been correlated with alpha-band power differences. The developmental trajectories of structural brain characteristics, such as gray matter volume, white matter volume, and cortical thickness, have been well-documented (Bethlehem et al., 2022). In future studies, these developmental trajectories of structural brain features could be related to the development trajectories of alpha-band waveform features to establish candidate structural contributors to changes in alpha-band waveform that can be tested more rigorously. Furthermore, these changes in resting-state alpha-band waveform features may reflect changes in cognitive abilities across development, given the implication of alpha rhythms in working memory (Foster et al., 2016; Jokisch and Jensen, 2007; Ede, 2018) and attention (Klimesch, 2012; Snyder and Foxe, 2010) and the improvements across development in working memory (Gathercole et al., 2004; Kwon, Reiss, and Menon, 2002) and attention (Luna et al., 2004; Rueda, Posner, and Rothbart, 2005).

Contrary to work implicating involving beta waveform shape in Parkinson's disease (Cole, van der Meij, et al., 2017), we found no significant differences in alpha-band rhythm features for either of two prominent neurodevelopmental disorders. This is consistent with recent work from Dede et al., 2023 that failed to find a single biomarker for ASD after extracting a high number of measures from resting-state EEG (in sensor space, including band-power and frequency measures) in a dataset of 776 individuals. There is large inter-individual variation in alpha-band rhythm features, but high internal consistency (Lopez et al., 2023), which hints at the fact that usage of longitudinal data (Gabard-Durnam et al., 2019) may be a promising approach to capture diagnosis-related information sufficiently. Our analysis suggests that it is challenging to use single-session resting-state oscillations for the construction of predictive biomarkers, but does not rule out that a more specific task-operationalization of deficits may be used to uncover disorder-specific physiology, e.g. in specialized motor or attentional paradigms (Vollebregt et al., 2016; Ter Huurne et al., 2017; Oberman et al., 2005). In summary, the need to go beyond resting-state analyses is highlighted here, in order to yield robust and reproducible results, which is a challenge in this context (Lefebvre et al., 2018).

Limitations

Given the heterogeneous data quality of a developmental EEG dataset, we made several design choices in our processing pipeline. First, we focused on high-SNR alpha-band rhythms, discarding any rhythms with SNR < 5 dB. The size of the dataset allowed us to be conservative in our rhythm classification while maintaining high statistical power for comparisons across the two rhythm types. Such stringent SNR criterion would severely limit the number of SSD components one could extract for other rhythms with lower SNR (e.g., beta rhythms) and might prove unnecessarily stringent for datasets that are inherently less noisy or have been more thoroughly preprocessed. Second, as shown in Fig. 1E, our pipeline identified a large number of parietal alpha-band rhythms. Occipital alpha and sensorimotor mu have well-established roles in modulation of sensory processing, while parietal alpha rhythms are modulated by attentional effort and only indirectly affect sensory processing (Sokoliuk et al., 2019). Given the hypotheses we aimed to test in this paper, we discarded the parietal alpha rhythms from our analysis, even though our results show that SSD could be used to identify parietal alpha rhythms in resting-state in future studies. Third, brain size changes substantially

during development and displays inter-individual variation, and we used a template brain averaged across ages 5–18. As such, our source localization procedure could have failed to properly localize components especially for the youngest and oldest children, whose brain sizes deviate most from the template brain used. Despite this concern, the distribution of identified components across age remained consistent with the participants' age distribution (top right of Fig. 1A). We also chose to include premotor areas and use a slightly larger ROI for the sensorimotor region to compensate for possible imprecision in the source localization. Fourth, because our primary hypotheses focused on waveform shape differences across age and diagnoses, we focused on across-participants analyses and looked only at the component with highest SNR for each rhythm type (occipital alpha and sensorimotor mu). The large number of participants allowed us to make high-powered statistical inferences even with this limitation. That said, future studies could use our spatial filtering approach to compare rhythms of the same type within participants, given that SSD is able to distinguish rhythms coming from the same cortical area in the same frequency band (Schaworonkow and Voytek, 2021a).

Conclusion

Occipital alpha rhythms and sensorimotor mu rhythms are difficult to disentangle in sensor-space EEG due to volume conduction, with occipital alpha dominating even the central channels. Using data-driven spatial filters, we extracted time series for alpha and mu components with high alpha SNR from a large developmental dataset. Analysis of the time series of these alpha-band components replicated findings of lower frequency and higher amplitude for alpha than for mu. We demonstrated that mu waveforms are more asymmetrical than alpha waveforms. We extended previous findings of alpha-band rhythms undergoing large changes in frequency during development, showing that these waveform shape measures also change substantially across development. While none of these resting-state changes appear to be associated with common neurodevelopmental disorders, characterizing differences across rhythm types remains vital for constraining generative models for alpha-band rhythms.

Materials and Methods

Experimental design

We analyzed an openly available dataset from the Healthy Brain Network project (Alexander et al., 2017). The Healthy Brain Network project by the Child Mind Institute is an ongoing initiative aiming to generate a large-scale, transdiagnostic sample for biomarker discovery and for investigations of the neural substrates associated with commonly occurring disorder phenotypes. In the following, we give a brief summary of the experimental methods focusing on the resting-state EEG components of the data collection which were used in this study, with full details regarding all acquired data (including fMRI data) given in the original publication.

Participants

Participants were recruited through advertisements that encouraged participation of families who had concerns about psychiatric symptoms in their child. These advertisements were distributed throughout the New York City metropolitan area. This recruitment strategy was developed with the main goal of the Healthy Brain Network–generating a large-scale, transdiagnostic sample–rather than the alternative of a fully representative epidemiologic design. Out of the 4245 participants listed in the first ten data releases we were able to successfully

download resting-state EEG data for 2969 participants, as resting-state EEG data acquisition was not conducted for all participants. To summarize the participant exclusion criteria (with description of the specific analysis steps following in subsequent paragraphs): we detected an alpha-band peak in at least one occipital or central channel in 2764 participants. 6 participants did not have an alpha peak in any of the 10 highest-SNR SSD components. 2216 participants had at least one source localized to alpha or mu regions, 1507 of these participants had sources that met the SNR and pattern distance thresholds and were used for subsequent analysis of waveform features. Of those, 1169 were male and 338 were female.

EEG recordings

High-density EEG data were recorded throughout the session in a sound-shielded room using a 128-channel EEG geodesic hydrocel system by Electrical Geodesics Inc. The data was recorded at the sampling rate of 500 Hz and was bandpass filtered between 0.1 and 100 Hz. The recording reference was at the vertex of the head (electrode Cz), and impedances were kept below 40 kOhms throughout the recording. The participants underwent a series of tasks in the session. For this paper, we analyzed data from the resting-state paradigm, in which participants alternated between viewing a fixation cross with their eyes open for 20 seconds and closing their eyes for 40 seconds for a total of five minutes. Data analysis was performed with Python using MNE-Python (version 1.1.0) (Gramfort et al., 2013). The analysis code needed to reproduce the analysis and figures is provided here: `http://github.com/nschawor/eeg-mu-alpha-development`.

Data preprocessing

For channel rejection, we used spherical spline interpolation for flat channels and for high-variance channels with a variance greater than three standard deviations away from the mean. We performed minimal preprocessing because SSD is able to separate components with high alpha SNR from the artifacts present in minimally processed EEG sensor data (Nikulin, Nolte, and Curio, 2011).

Calculation of spectral parameterization

To calculate power spectra from the extracted time series, we used Welch's method (window length: 4 seconds, 0% overlap, Hamming window). We then used the spectral parameterization toolbox (version 1.0.0) (Donoghue et al., 2020) for the calculation of alpha oscillatory power and aperiodic exponents. The power spectrum is modeled as a combination of aperiodic and oscillatory components, which allows for isolation of alpha oscillatory power from aperiodic components. The power spectral density $P(f)$ for each frequency f is expressed as:

$$P(f) = L(f) + \sum_n G_n(f), \tag{1}$$

with the aperiodic contribution $L(f)$ expressed as:

$$L(f) = b - \log[f^{\chi}], \tag{2}$$

with a constant offset b and the aperiodic exponent χ. When the power spectrum is plotted on a log-log axis, the aperiodic exponent χ corresponds to the slope of a line. Each oscillatory contribution $G_n(f)$ is modeled as a Gaussian peak:

$$G_n(f) = a \exp\left[-\frac{(f-\mu_n)^2}{2\sigma_n^2}\right], \tag{3}$$

with a as the amplitude, μ_n as the center frequency and σ_n as the bandwidth of each component. The number of oscillatory components is determined from the data, with the option to set a maximum number of components as a parameter. The general model assumption here is that oscillatory and aperiodic processes are distinct and separable. Parameters for spectral parameterization were set as follows: peak width limits: (1, 12); maximum number of peaks: 5; minimum peak amplitude exceeding the aperiodic fit: 0.0; peak threshold: 2.0; and aperiodic mode: 'fixed'.

We first used spectral parameterization to find the peak frequency in the 6–13 Hz range for two occipital (E70 and E83) and two sensorimotor channels (E36 and E104) after computing the spatial Laplacian for these channels. This was done to get an approximate estimate of the peak frequencies for alpha and for mu rhythms in each participant to be used as a parameter in the spatial filter calculation described below. 2764 of the 2969 participants for which we were able to successfully download their EEG data had an alpha peak in at least one of the four selected channels. After alpha and mu components were identified, spectral parameterization was again applied to determine the peak frequency for each component. The aperiodic component was not used for any subsequent analyses, as the spatial filtering only optimizes for extracting oscillations and the effects of this procedure on the aperiodic exponent are not known.

Calculation of spatial filters and patterns

For extracting rhythms in the alpha-band, we used spatio-spectral decomposition (SSD) (Nikulin, Nolte, and Curio, 2011). SSD maximizes spectral power in a frequency band of interest while minimizing spectral power in flanking frequency bands, thus enhancing the height of spectral peaks over the aperiodic component and exploiting the typical narrowband peak structure of neural rhythms (see Fig. 1C). Because alpha peak frequency can vary widely across participants, we used the average alpha peak frequency from spectral parameterization for each participant (α_{freq}) as the center frequency for the SSD frequency band of interest. SSD models the measured time series $\mathbf{X}$ (a matrix with t samples and k electrodes) as a linear combination of signal $\mathbf{X_S}$ and noise $\mathbf{X_N}$:

$$\mathbf{X} = \mathbf{X_S} + \mathbf{X_N}. \tag{4}$$

In our case, the signal $\mathbf{X_S}$ is the signal in the alpha band, while the noise $\mathbf{X_N}$ is the signal in the neighboring frequency bands. $\mathbf{X_S}$ was calculated by bandpass filtering $(\alpha_{\text{freq}} - 2, \alpha_{\text{freq}} + 2)$. Following the procedure of (Nikulin, Nolte, and Curio, 2011), $\mathbf{X_N}$ was calculated by bandpass filtering $(\alpha_{\text{freq}} - 4, \alpha_{\text{freq}} + 4)$ and then bandstop filtering $(\alpha_{\text{freq}} - 3, \alpha_{\text{freq}} + 3)$. We can then calculate the signal covariance $\mathbf{C_S}$ and noise covariance $\mathbf{C_N}$ from the corresponding time series:

$$\mathbf{C_S} = \mathbf{X_S}^T \mathbf{X_S}; \tag{5}$$

$$\mathbf{C_N} = \mathbf{X_N}^T \mathbf{X_N}. \tag{6}$$

We aim to find spatial filters $\mathbf{W}$ that maximize the power of the projected signal P_S while minimizing the power of the projected noise P_N:

$$\text{SNR}(\mathbf{W}) = \frac{P_S}{P_N} = \frac{\text{var}(\mathbf{W}^T\mathbf{X_S})}{\text{var}(\mathbf{W}^T\mathbf{X_N})} = \frac{\mathbf{W}^T\mathbf{C_S}\mathbf{W}}{\mathbf{W}^T\mathbf{C_N}\mathbf{W}}. \tag{7}$$

We can then transform this Rayleigh quotient into the following generalized eigenvalue problem:

$$\mathbf{C_S} = \mathbf{C_N}\mathbf{W}\mathbf{\Lambda}, \tag{8}$$

where $\mathbf{\Lambda}$ is the unity matrix with the corresponding eigenvalues on the diagonal. Each column of $\mathbf{W}$ is a spatial filter, and each participant will have as many spatial filters as electrodes (i.e., k spatial filters), with the spatial filters ordered by relative SNR in the frequency band of interest. Time series for each SSD component can be obtained from broadband activity across electrodes through matrix multiplication of the transposed spatial filters:

$$\hat{\mathbf{S}} = \mathbf{W^T}\mathbf{X}. \tag{9}$$

Crucially, because the SSD component time series is a linear transformation on the broadband activity rather than filtered activity, nonsinusoidal features of the waveforms, such as harmonics, are retained in the SSD component time series, allowing for fine-grained analysis of waveform shape. Finally, we can determine the spatial patterns $\mathbf{A}$ for each participant by inverting the matrix of spatial filters:

$$\mathbf{A} = \mathbf{W}^{-1}. \tag{10}$$

These spatial patterns can then be used to interpret the spatial origin of the extracted SSD components (Schaworonkow and Voytek, 2021a), and in our case, classify the SSD components as occipital alpha or sensorimotor mu (see below).

Classifying alpha rhythms as occipital alpha and sensorimotor mu

To estimate source locations for each component, we computed the leadfield from a pediatric template brain and found the source that best accounts for that component's spatial pattern. We first averaged the age-appropriate atlas from Fonov and colleagues (Fonov et al., 2011) over ages 4.5 to 18.5 years and used this as our template head and brain model. We then segmented the template head into the inner skull, outer skull, and outer skin surfaces and used these surfaces to create a 3-layer Boundary Element Method (BEM) model using FreeSurfer (Fischl, 2012). We aligned the FreeSurfer surfaces and BEM model to the template electrode positions. Next, we created a surface-based source space with a recursively subdivided octahedron. We computed the forward solution using the BEM model and surface-based source spaces, giving us a spatial pattern for each dipole source. Finally, we computed the cosine distance between each component's spatial pattern and the spatial patterns generated by each dipole. The dipole with the lowest cosine distance was then defined as the source location for that component.

Using the HCP-MMP1 parcellation (Glasser et al., 2016), components that were localized to the occipital cortex were classified as alpha components and those that were localized to somatosensory, motor, premotor, paracentral lobular, and midcingulate cortices were classified as mu components. 2216 participants had at least one component with a source classified as mu or alpha according to spatial location. For waveform shape analyses, we excluded components with SNR <= 5 dB and spatial pattern distance >= 0.15 from the best dipole to ensure that the components are strong alpha sources with well-estimated source locations. 1507 participants had at least one alpha or mu component that passed these SNR and spatial pattern distance thresholds. To simplify comparisons across participants, we only used each participant's highest-SNR alpha component and highest-SNR mu component in further analyses.

Calculation of waveform measures

For all of the alpha and mu components, we then calculated measures of waveform shape from the component time series using the bycycle package (version 1.0.0) (Cole and Voytek, 2019). This complementary approach to spectral analyses allows us to examine the nonsinusoidal, asymmetric features of the alpha and mu rhythms. First, we filtered the component time series in the broad frequency band from 1–45 Hz to remove slow drifts as well as high frequency noise that would complicate extrema localization without deforming the shape of the alpha and mu rhythms. To extract the time points of zero crossings, the time series is then narrowband filtered at the component peak frequency identified earlier using spectral parameterization +/- 2 Hz. Next, the peaks and troughs for each cycle are extracted by finding the absolute maxima and minima of the broadband signal between the zero-crossing time points. The rise and decay were defined as the phase from trough to peak and the phase from peak to trough, respectively. Because oscillations are infrequent and bursty (Cole and Voytek, 2019; Jones, 2016; Lundqvist et al., 2016), we next performed burst detection to determine which individual cycles represent alpha and mu bursts. Burst detection parameters were set as follows for all components: amplitude fraction threshold: 0.5 (cycles with amplitudes smaller than the median amplitude were discarded), amplitude consistency threshold: 0.5 (cycles where the difference in rise and decay voltage values was greater than the median difference were discarded), period consistency threshold: 0.5 (cycles where the difference between the cycle period and the period of neighboring cycles was greater than the median were discarded), monotonicity threshold: 0.5 (cycles where the fraction of instantaneous voltage changes between consecutive samples that are positive during rise and negative during the decay phase was smaller than 0.5 were discarded). These relatively stringent burst criteria have been used previously to investigate waveform shape of low-frequency bursts in infants (Schaworonkow and Voytek, 2021b). We determined the cycle frequency, rise-decay asymmetry, peak-trough asymmetry, and cycle amplitude from the times and voltages of the extracted critical points for each cycle as follows:

- frequency: $f = \frac{1}{t_{\text{trough,cycle}_{n+1}} - t_{\text{trough,cycle}_n}}$
- rise-decay asymmetry: $\text{asym}_{\text{rd}} = |\frac{t_{\text{rise}}}{t_{\text{rise}} + t_{\text{decay}}} - 0.5|$
- peak-trough asymmetry: $\text{asym}_{\text{pt}} = |\frac{t_{\text{peak}}}{t_{\text{peak}} + t_{\text{trough}}} - 0.5|$
- amplitude: $\text{amp} = \frac{v_{\text{rise}} + v_{\text{decay}}}{2}$. To account for any unequal voltage scaling across components from SSD, we normalized the cycle amplitude across each component by dividing the amplitude of cycles within bursts by the average amplitude of all cycles from non-bursts.

Statistical analysis

Statistical analyses were carried out using the pingouin Python package (version 0.5.3) (Vallat, 2018). We used t-tests to determine if there were significant differences in waveform features between alpha and mu (Fig. 2). We evaluated the effect sizes of these contrasts using Cohen's d. In order to determine whether the waveform features change across development for alpha and mu, we first calculated correlation coefficients across age for each rhythm type (Fig. 3A). To assess whether the waveform features change differently by rhythm type, we used permutation statistics and linear models to bootstrap the slope and offset for each waveform feature of each rhythm type. Specifically, we resampled feature values with replacement and fit a linear model for each rhythm type in which each feature is a function of age: feature = $\beta_1 \cdot \text{age} + \beta_0$, giving us bootstrapped distributions of slope (β_1) and offset (β_0) for each waveform feature and rhythm type (Fig. 3B and 3C). We then calculated p-values for differences in the β coefficients between rhythm types by comparing the percentage of bootstraps where the difference of the β coefficient of alpha and mu was either above or below zero to 50%. Finally, we evaluated whether waveform shape features differ across clinical diagnoses (Fig. 4), independent of the observed changes in these waveform features with age, by performing an ANCOVA and using age as a covariate. We performed post-hoc t-tests on the residuals obtained from the linear regression of age with each waveform feature. This analysis aimed to verify pairwise non-significance in line with the results of the ANCOVA. All reported p-values were corrected for multiple comparisons using the Bonferroni correction, except in the case of relating waveform features to diagnoses, where we used the Benjamini-Hochberg procedure (Benjamini and Hochberg, 1995) to decrease the chance of Type II errors (i.e., falsely claim that there are no significant differences in waveform features across diagnoses when there are).

References

Alexander, LM et al. (2017). "An open resource for transdiagnostic research in pediatric mental health and learning disorders". In: *Scientific Data* 4.1, pp. 170–181. DOI: 10.1038/sdata.2017.181.

Benjamini, Y and Hochberg, Y (1995). "Controlling the false discovery rate: a practical and powerful approach to multiple testing". In: *Journal of the Royal statistical society: series B (Methodological)* 57.1, pp. 289–300.

Berger, H (1929). "Über das Elektrenkephalogramm des Menschen". In: *Archiv für Psychiatrie und Nervenkrankheiten.*

Bethlehem, RAI et al. (2022). "Brain charts for the human lifespan". In: *Nature* 604.7906, pp. 525–533. DOI: 10.1038/s41586-022-04554-y.

Cellier, D, Riddle, J, Petersen, I, and Hwang, K (2021). "The development of theta and alpha neural oscillations from ages 3 to 24 years". In: *Developmental cognitive neuroscience* 50, p. 100969.

Cole, SR, van der Meij, R, Peterson, EJ, Hemptinne, C de, Starr, PA, and Voytek, B (2017). "Nonsinusoidal Beta Oscillations Reflect Cortical Pathophysiology in Parkinson's Disease". In: *The Journal of Neuroscience* 37.18, pp. 4830–4840. DOI: 10.1523/JNEUROSCI.2208-16.2017.

Cole, SR and Voytek, B (2017). "Brain Oscillations and the Importance of Waveform Shape". In: *Trends in Cognitive Sciences* 21.2, pp. 137–149. DOI: 10.1016/j.tics.2016.12.008.

Cole, SR and Voytek, B (2019). "Cycle-by-cycle analysis of neural oscillations". In: *Journal of Neurophysiology* 122.2, pp. 849–861. DOI: 10.1152/jn.00273.2019.

Dede, AJ, Xiao, W, Vaci, N, Cohen, MX, and Milne, E (2023). "Lack of univariate, clinically-relevant biomarkers of autism in resting state EEG: a study of 776 participants". In: *medRxiv*. DOI: 10.1101/2023.05.21.23290300.

Donoghue, T et al. (2020). "Parameterizing neural power spectra into periodic and aperiodic components". In: *Nature Neuroscience* 23.12, pp. 1655–1665. DOI: 10.1038/s41593-020-00744-x.

Dumas, G, Soussignan, R, Hugueville, L, Martinerie, J, and Nadel, J (2014). "Revisiting mu suppression in autism spectrum disorder". In: *Brain research* 1585, pp. 108–119.

Ede, F van (2018). "Mnemonic and attentional roles for states of attenuated alpha oscillations in perceptual working memory: a review". In: *The European Journal of Neuroscience* 48.7, pp. 2509–2515. DOI: 10.1111/ejn.13759.

Fischl, B (2012). "FreeSurfer". In: *NeuroImage* 62.2, pp. 774–781. DOI: 10.1016/j.neuroimage.2012.01.021.

Fonov, V, Evans, AC, Botteron, K, Almli, CR, McKinstry, RC, and Collins, DL (2011). "Unbiased average age-appropriate atlases for pediatric studies". In: *NeuroImage* 54.1, pp. 313–327. DOI: 10.1016/j.neuroimage.2010.07.033.

Foster, JJ, Sutterer, DW, Serences, JT, Vogel, EK, and Awh, E (2016). "The topography of alpha-band activity tracks the content of spatial working memory". In: *Journal of Neurophysiology* 115.1, pp. 168–177. DOI: 10.1152/jn.00860.2015.

Freschl, J, Azizi, LA, Balboa, L, Kaldy, Z, and Blaser, E (2022). "The development of peak alpha frequency from infancy to adolescence and its role in visual temporal processing: A meta-analysis". In: *Developmental Cognitive Neuroscience* 57, p. 101146. DOI: 10.1016/j.dcn.2022.101146.

Gabard-Durnam, LJ, Wilkinson, C, Kapur, K, Tager-Flusberg, H, Levin, AR, and Nelson, CA (2019). "Longitudinal EEG power in the first postnatal year differentiates autism outcomes". In: *Nature communications* 10.1, p. 4188.

Gastaut, HJ and Bert, J (1954). "EEG changes during cinematographic presentation (Moving picture activation of the EEG)". In: *Electroencephalography and Clinical Neurophysiology* 6, pp. 433–444. DOI: 10.1016/0013-4694(54)90058-9.

Gathercole, SE, Pickering, SJ, Ambridge, B, and Wearing, H (2004). "The structure of working memory from 4 to 15 years of age". In: *Developmental Psychology* 40.2, pp. 177–190. DOI: 10.1037/0012-1649.40.2.177.

Glasser, MF et al. (2016). "A multi-modal parcellation of human cerebral cortex". In: *Nature* 536.7615, pp. 171–178.

Gramfort, A et al. (2013). "MEG and EEG data analysis with MNE-Python". In: *Frontiers in Neuroscience* 7. DOI: 10.3389/fnins.2013.00267.

Halgren, M et al. (2019). "The generation and propagation of the human alpha rhythm". In: *Proceedings of the National Academy of Sciences* 116.47, pp. 23772–23782. DOI: 10.1073/pnas.1913092116.

Jansen, BH and Rit, VG (1995). "Electroencephalogram and visual evoked potential generation in a mathematical model of coupled cortical columns". In: *Biol. Cybern.* 73, pp. 357–366.

Javitt, DC et al. (2020). "A roadmap for development of neuro-oscillations as translational biomarkers for treatment development in neuropsychopharmacology". In: *Neuropsychopharmacology* 45.9, pp. 1411–1422. DOI: 10.1038/s41386-020-0697-9.

Jokisch, D and Jensen, O (2007). "Modulation of gamma and alpha activity during a working memory task engaging the dorsal or ventral stream". In: *The Journal of Neuroscience: The Official Journal of the Society for Neuroscience* 27.12, pp. 3244–3251. DOI: 10.1523/JNEUROSCI.5399-06.2007.

Jones, SR (2016). "When brain rhythms aren't 'rhythmic': implication for their mechanisms and meaning". In: *Current Opinion in Neurobiology* 40, pp. 72–80. DOI: 10.1016/j.conb.2016.06.010.

Kelly, SP, Lalor, EC, Reilly, RB, and Foxe, JJ (2006). "Increases in Alpha Oscillatory Power Reflect an Active Retinotopic Mechanism for Distracter Suppression During Sustained Visuospatial Attention". In: *Journal of Neurophysiology* 95.6, pp. 3844–3851. DOI: 10.1152/jn.01234.2005.

Klimesch, W (2012). "Alpha-band oscillations, attention, and controlled access to stored information". In: *Trends in Cognitive Sciences* 16.12, pp. 606–617. DOI: 10.1016/j.tics.2012.10.007.

Kuhlman, WN (1978). "Functional topography of the human mu rhythm". In: *Electroencephalography and Clinical Neurophysiology* 44.1, pp. 83–93. DOI: 10.1016/0013-4694(78)90107-4.

Kwon, H, Reiss, AL, and Menon, V (2002). "Neural basis of protracted developmental changes in visuo-spatial working memory". In: *Proceedings of the National Academy of Sciences of the United States of America* 99.20, pp. 13336–13341. DOI: 10.1073/pnas.162486399.

Lefebvre, A et al. (2018). "Alpha waves as a neuromarker of autism spectrum disorder: the challenge of reproducibility and heterogeneity". In: *Frontiers in neuroscience* 12, p. 662.

Lindsley, DB (1939). "A Longitudinal Study of the Occipital Alpha Rhythm in Normal Children: Frequency and Amplitude Standards". In: *The Pedagogical Seminary and Journal of Genetic Psychology* 55.1, pp. 197–213. DOI: 10.1080/08856559.1939.10533190.

Lopes Da Silva, F, Van Rotterdam, A, Barts, P, Van Heusden, E, and Burr, W (1976). "Models of Neuronal Populations: The Basic Mechanisms of Rhythmicity". In: *Progress in Brain Research*. Vol. 45. Elsevier, pp. 281–308. ISBN: 978-0-444-41457-1. DOI: 10.1016/S0079-6123(08)60995-4.

Lopez, K, Monachino, A, Vincent, K, Peck, F, and Gabard-Durnam, L (2023). "Stability, change, and reliable individual differences in electroencephalography measures: a lifespan perspective on progress and opportunities". In: *NeuroImage*, p. 120116.

Luna, B, Garver, KE, Urban, TA, Lazar, NA, and Sweeney, JA (2004). "Maturation of cognitive processes from late childhood to adulthood". In: *Child Development* 75.5, pp. 1357–1372. DOI: 10.1111/j.1467-8624.2004.00745.x.

Lundqvist, M, Rose, J, Herman, P, Brincat, SL, Buschman, TJ, and Miller, EK (2016). "Gamma and Beta Bursts Underlie Working Memory". In: *Neuron* 90.1, pp. 152–164. DOI: 10.1016/j.neuron.2016.02.028.

Nikulin, VV, Nolte, G, and Curio, G (2011). "A novel method for reliable and fast extraction of neuronal EEG/MEG oscillations on the basis of spatio-spectral decomposition". In: *NeuroImage* 55.4, pp. 1528–1535. DOI: 10.1016/j.neuroimage.2011.01.057.

Oberman, LM, Hubbard, EM, McCleery, JP, Altschuler, EL, Ramachandran, VS, and Pineda, JA (2005). "EEG evidence for mirror neuron dysfunction in autism spectrum disorders". In: *Cognitive Brain Research* 24.2, pp. 190–198. DOI: 10.1016/j.cogbrainres.2005.01.014.

Pfurtscheller, G and Neuper, C (1994). "Event-related synchronization of mu rhythm in the EEG over the cortical hand area in man". In: *Neuroscience Letters* 174.1, pp. 93–96. DOI: 10.1016/0304-3940(94)90127-9.

Rueda, MR, Posner, MI, and Rothbart, MK (2005). "The development of executive attention: contributions to the emergence of self-regulation". In: *Developmental Neuropsychology* 28.2, pp. 573–594. DOI: 10.1207/s15326942dn2802_2.

Salmelin, R and Hari, R (1994). "Spatiotemporal characteristics of sensorimotor neuromagnetic rhythms related to thumb movement". In: *Neuroscience* 60.2, pp. 537–550. DOI: 10.1016/0306-4522(94)90263-1.

Schaworonkow, N and Nikulin, VV (2022). "Is sensor space analysis good enough? Spatial patterns as a tool for assessing spatial mixing of EEG/MEG rhythms". In: *NeuroImage* 253. DOI: 10.1016/j.neuroimage.2022.119093..

Schaworonkow, N and Voytek, B (2021a). "Enhancing oscillations in intracranial electrophysiological recordings with data-driven spatial filters". In: *PLOS Computational Biology* 17.8. Ed. by D Marinazzo, e1009298. DOI: 10.1371/journal.pcbi.1009298.

Schaworonkow, N and Voytek, B (2021b). "Longitudinal changes in aperiodic and periodic activity in electrophysiological recordings in the first seven months of life". In: *Developmental Cognitive Neuroscience* 47, p. 100895. DOI: 10.1016/j.dcn.2020.100895.

Sherman, MA et al. (2016). "Neural mechanisms of transient neocortical beta rhythms: Converging evidence from humans, computational modeling, monkeys, and mice". In: *Proceedings of the National Academy of Sciences* 113.33, E4885–E4894. DOI: 10.1073/pnas.1604135113.

Snyder, AC and Foxe, JJ (2010). "Anticipatory Attentional Suppression of Visual Features Indexed by Oscillatory Alpha-Band Power Increases:A High-Density Electrical Mapping Study". In: *Journal of Neuroscience* 30.11, pp. 4024–4032. DOI: 10.1523/JNEUROSCI.5684-09.2010.

Sokoliuk, R et al. (2019). "Two Spatially Distinct Posterior Alpha Sources Fulfill Different Functional Roles in Attention". In: *The Journal of Neuroscience* 39.36, pp. 7183–7194. DOI: 10.1523/JNEUROSCI.1993-18.2019.

Stam, C, Pijn, J, Suffczynski, P, and Lopes da Silva, F (1999). "Dynamics of the human alpha rhythm: evidence for non-linearity?" In: *Clinical Neurophysiology* 110.10, pp. 1801–1813. DOI: 10.1016/S1388-2457(99)00099-1.

Ter Huurne, N, Lozano-Soldevilla, D, Onnink, M, Kan, C, Buitelaar, J, and Jensen, O (2017). "Diminished modulation of preparatory sensorimotor mu rhythm predicts attention-deficit/hyperactivity disorder severity". In: *Psychological Medicine* 47.11, pp. 1947–1956.

Thut, G, Nietzel, A, Brandt, SA, and Pascual-Leone, A (2006). "Alpha-Band Electroencephalographic Activity over Occipital Cortex Indexes Visuospatial Attention Bias and Predicts Visual Target Detection". In: *Journal of Neuroscience* 26.37, pp. 9494–9502. DOI: 10.1523/JNEUROSCI.0875-06.2006.

Vallat, R (2018). "Pingouin: statistics in Python". In: *Journal of Open Source Software* 3.31, p. 1026. DOI: 10.21105/joss.01026.

Vollebregt, MA, Zumer, JM, Ter Huurne, N, Buitelaar, JK, and Jensen, O (2016). "Posterior alpha oscillations reflect attentional problems in boys with Attention Deficit Hyperactivity Disorder". In: *Clinical Neurophysiology* 127.5, pp. 2182–2191. DOI: 10.1016/j.clinph.2016.01.021.

Worden, MS, Foxe, JJ, Wang, N, and Simpson, GV (2000). "Anticipatory Biasing of Visuospatial Attention Indexed by Retinotopically Specific α-Bank Electroencephalography Increases over Occipital Cortex". In: *The Journal of Neuroscience* 20.6, RC63–RC63. DOI: 10.1523/JNEUROSCI.20-06-j0002.2000.